Selective Electrocatalytic Nitrate Reduction to Ammonia using Nafion-covered Cu Electrodeposits

Profulla Mondol, Jashmeen K. Thind, and Christopher J. Barile*

Corresponding Author

Christopher J. Barile - *Department of Chemistry, University of Nevada, Reno, Reno, NV 89557, USA; orcid.org/0000-0002-4893-9506*; Email: cbarile@unr.edu

Authors

Profulla Mondol- *Department of Chemistry, University of Nevada, Reno, Reno, NV 89557, USA*

Jashmeen K. Thind- *Department of Chemistry, University of Nevada, Reno, Reno, NV 89557, USA*

Abstract

Electrocatalytic NH_3 production from NO_3^- reduction is a promising alternative to traditional Haber-Bosch NH_3 synthesis. Although Nafion is commonly employed as a separator in two-compartment electrochemical cells and as a binder in catalyst inks, in this manuscript, we use Nafion as an overlayer on top of Cu electrodeposits to enhance NH_3 selectivity. Faradaic efficiencies for NH_3 and NO_2^- generation were evaluated as a function of electrodeposit morphology with and without the Nafion layer. These studies reveal that the combination of Cu (220) faces in the electrodeposits and activation of a NO intermediate by Nafion enables NH_3 production with a high Faradaic efficiency of (97.0 ± 0.3) %. This optimized architecture also exhibits the fastest rate of NH_3 production among the catalysts studied even after normalizing for its rough electrochemical active surface area. In addition to voltammetry, the electrocatalysts were characterized using a variety of techniques including atomic force microscopy, scanning electron microscopy, X-ray diffraction, and water contact angle measurements. Insights garnered about the parameters needed for selective NH_3 production will inform future research on non-precious metal NO_3^- reduction catalysts.

Keywords: Nitrate reduction, electrocatalysis, ammonia production, Nafion, catalyst selectivity

Introduction

Nitrate (NO_3^-) conversion or removal is important to balance the nitrogen cycle in the environment. NO_3^- is a common pollutant from agricultural runoff and other industrial activities that has caused a misbalance in the natural nitrogen cycle. Excess NO_3^- is responsible for toxic algae blooms in waterways and also poses human health concerns.[1] For these reasons, the conversion of NO_3^- into other products is of great research interest.[2–5]

As the most important chemical in the nitrogen fertilizer industry, ammonia (NH_3) is a value-added product attainable from electrocatalytic NO_3^- reduction.[6–10] In fact, NH_3 is currently the fifth most produced chemical by volume in the world.[11] Because the Haber-Bosch process used to synthesize NH_3 is energy intensive and responsible for 1-2% of anthropogenic CO_2 production, alternative routes to generating NH_3 are needed.[12–15] Thus, electrocatalytic NO_3^- reduction to NH_3 is a potential pathway to both increase energy efficiency and remove environmental NO_3^- contamination. However, a major hurdle facing electrocatalytic NO_3^- reduction technology is poor catalyst selectivity. In particular, converting NO_3^- to NH_3 ($NO_3^- + 9\ H^+ + 8\ e^- \rightarrow NH_3 + 3H_2O$) requires the transfer of 9 H^+ and 8 e^-, and side products can be generated during this multistep process, which decreases the Faradaic efficiency of NH_3 production.[1,16–20]

To increase the catalyst activity and selectivity, researchers have explored various electrocatalysts including noble metal catalysts, transition metals, alloys, and non-metallic electrodes.[1,21–26] Among them, Cu-based catalysts have been emphasized due to their excellent NO_3^- adsorption properties.[5,27,28] For example, Kang et al. developed structure-activity relationships between different Cu materials including Cu nanosheets, nanocubes, nanoparticles, and foils.[27] Zhang et al. unveiled the active phase of Cu-based electrocatalysts and demonstrated that Cu/Cu_2O turns into CuO during NO_3^- reduction, which facilitates the formation of a *NOH

intermediate and suppresses the H_2 evolution reaction.[5] Many reports have developed Cu catalysts with a second metal such as Ni or Pd, which significantly increase NH_3 production due to modulated electronic structure and synergistic effects.[22,29]

The fluoropolymer Nafion is commonly used as a separator between the two half compartments in full electrochemical devices and as a binder in catalyst inks.[30,31] Recently, our group used Nafion in a different manner to increase the selectivity of NH_3 production from NO_3^- on flat polycrystalline metal electrodes in which a Nafion overlayer covered the electrocatalysts.[32] Surface-enhanced Raman spectroscopy and density functional theory calculations indicate that the metal-NO intermediate is activated in the presence of the Nafion layer. In this article, we expand upon this work by developing NO_3^- reduction catalysts using Nafion-modified Cu electrodeposits that display both enhanced current densities and NH_3 selectivities. We elucidate the physical and chemical parameters that give rise to this enhanced performance.

Methods

General Procedures

A Nafion D520 dispersion was obtained from Fuel Cell Store, Inc. Cu foil (99.99%) was obtained from All-Foils, Inc. and was sonicated 8 min in acetone and 10 min in deionized water successively before use. $NaNO_3$ (> 99%) and Na_2SO_4 (> 99%) were procured from Sigma Aldrich, while $NaNO_2$ (98%) was purchased from Oakwood Chemicals, Inc. KH_2PO_4 and $Ru(NH_3)_6Cl_3$ were obtained from Fischer Scientific. Cu electrodeposits were formed on Cu foil using chronoamperometry for 30 min in 0.8 M $CuSO_4$ and 1 M H_2SO_4 solution at either -0.14 V or -0.5 V using a three-electrode electrochemical cell with the Cu foil serving as the working electrode, a leakless Ag/AgCl/ 3 M KCl (eDaq, Inc.) reference electrode, and a Pt wire counter electrode. After washing with water, the electrodeposited electrode was dried at room

temperature in air overnight. Nafion-modified electrodes were fabricated by drop-casting the Nafion dispersion directly on each side of the electrodeposited Cu surfaces. Each side of the Nafion film was dried at room temperature for 15 min before use. The thickness of the Nafion was modulated by using multiple rounds of dropcasting and drying.

Electrochemical Measurements

Electrochemical studies were performed using a VSP-300 Biologic potentiostat. A three-electrode system was used with modified Cu surfaces, a Pt-coated Ti mesh electrode (Rio Grande, Inc.), and a leakless Ag/AgCl/ 3 M KCl (eDaq, Inc.) electrode were used as working, counter, and reference electrodes, respectively for all electrochemical experiments unless mentioned otherwise. All electrochemical potentials were reported with respect to a Ag/AgCl reference electrode. Current densities are calculated with respect to the electrochemically active surface area of the working electrodes. The electrochemically active surface areas of the electrodes were obtained by performing cyclic voltammetry (CV) in a 0.1 M pH 7.0 phosphate buffer solution containing 1 mM $Ru(NH_3)_6Cl_3$ from -0.1 V to 0.5 V at 50 mV/s in a one compartment cell (Figure S1). The second cycle of each CV was used to calculate the electrochemical surface area by integrating the charge under the Ru^{2+} to Ru^{3+} couple. The integrated charge for each surface was then compared to the integrated charge for a flat Cu electrode to determine the electrochemically active surface area.

A two-compartment cell containing 10 mL of 50 mM $NaNO_3$ and 100 mM Na_2SO_4 was used for studying NO_3^- reduction activities for different working electrodes. The Pt-coated Ti counter electrode was put in one compartment, which was separated from the working and reference electrodes by a Nafion 117 membrane (183 μm thick, Fuel Cell Store, Inc.). This membrane prevents possible reoxidation of NO_3^- reduction products formed on the working

electrode by the positive potential of the counter electrode. For all linear sweep voltammetry (LSV) experiments, onset potentials were calculated by determining the voltage at which 10% of the maximum current density was attained.

For electrochemical NO_2^- reduction studies, an electrolyte containing 50 mM $NaNO_2$ and 100 mM Na_2SO_4 in a two-compartment cell was used following a procedure analogous to NO_3^- reduction. For electrochemical NO reduction, the electrolyte consisted of 100 mM Na_2SO_4 and was sparged with NO gas for 10 minutes before conducting electrochemistry in a two-compartment cell. NO gas was prepared from $NaNO_2$ and 1 M H_2SO_4 following literature procedures.[33] The produced NO_x species were washed with NaOH, which absorbs acidic NO_2, resulting in a NO stream. The NO concentration in solution before electrochemistry was 2 mM.[34]

Materials Characterization

Scanning electron microscope (SEM) images and energy-dispersive X-ray (EDX) analysis were obtained using a JEOL JSM-7100F field emission SEM operated using an accelerating voltage of 15 kV. Atomic force microscopy (AFM) images were obtained for each sample using a Nanosurf EasyScan 2 microscope operated in contact mode using a silicon tip with an aluminum reflective coating (ContAl-G, TedPella, Inc.). A Rame-Hart 100-00 goniometer was used to measure contact angles. 20 μL of distilled water was placed on each electrode surface using a micropipette. The contact angles were measured at room temperature within 5 s of dispensing the water droplet. Reported contact angles are calculated from the average of the left and right angles of the droplet, and each measurement was conducted three times. X-ray diffraction (XRD) data was collected with a Bruker D2 X-ray diffractometer.

Product Detection

Standard colorimetric methods were used to detect the concentration of NH_3, NO_2^-, and NO_3^- after chronoamperometry. The amount of NH_3 was quantified using the indophenol method.[35] Required reagents were purchased from Sigma Aldrich and used without further purification. In a typical preparation, 0.5 mL of the catholyte was taken in a glass vial, and 2 mL of a 1 M NaOH solution containing 5 wt. % salicylic acid and 5 wt. % sodium citrate was added. Then, 1 mL of 0.05 M NaClO and 0.2 mL of 1 wt. % sodium nitroferricyanide were added to the same vial. After this mixture was let to stand at 2 h at 4°C, UV-Vis spectroscopy was performed using a Shimadzu UV-2550 spectrometer. The concentration of NH_3 in the electrolyte was determined using the maximum absorbance at 670 nm along with an appropriate calibration curve produced using NH_3 solutions of known concentrations.

Griess reagents with and without VCl_3 were used to quantify the NO_3^- and NO_2^-, respectively.[36] The Griess reagent was first prepared by dissolving 2 wt. % NEDD (N-(1-naphthyl)ethylenediamine dihydrochloride) and 2 wt. % sulfanilamide in 200 mL of 0.5 M HCl solution.

10 μL of the catholyte was diluted with 2 mL water in a glass vial to quantify NO_2^- concentration. 0.8 mL of the Griess reagent was added in that vial, and the mixture was let to stand for 2 h at room temperature to allow the reaction to go to completion. The absorbance at 540 nm was used to calculate the NO_2^- concentration using an appropriate calibration curve constructed from NO_2^- solutions of known concentrations.

To calculate the amount of NO_3^- consumed after chronoamperometry, 5 μL of the catholyte was diluted with 2 mL of water. Then, 200 mL of the Griess reagents solution was made as described previously, and 0.5 g VCl_3 was added. 0.8 mL of this solution was added to the above mixture, and it was let to stand overnight at room temperature to allow the reaction to

go to completion. NO_3^- is reduced to NO_2^- in the presence of VCl_3 and that total NO_2^- concentration was quantified using UV-Vis spectroscopy using the maximum absorbance at 540 nm. The total NO_2^- concentration was subtracted from the above NO_2^- concentration to determine the unconverted NO_3^- during chronoamperometry.

Faradaic Efficiency Calculations

Faradaic efficiency (% FE) values of NH_3 and NO_2^- production were calculated using the established procedures.[32] The catalysts studied in this project did not yield any measurable quantities (Faradaic efficiency > 0.1%) of N_2, NO, N_2O, or N_2H_4 as determined by previously described methods.[32] Faradaic efficiency for H_2 production was not explicitly reported, but it can be found by subtracting the Faradaic efficiency for all nitrogen-containing products from 100%.

Results and Discussion

Surface Characterization of Electrocatalysts

Figure 1 presents top-down SEM images of Cu electrodes modified with Cu electrodeposits produced using 30 min of electrodeposition at either -0.14 V or -0.5 V from a Cu electrodeposition bath. While the electrodeposits formed at -0.14 V are relatively smooth (Figures 1A and 1B), when the electrodeposits are formed using -0.5 V, the surface consists of large particles (> 10 μm) in a three-dimensional agglomerate-like structure (Figures 1C and 1D). Electrodeposition at higher overpotentials is known to give rise to larger particles sizes in many other contexts.[37] To understand further the surface morphology of the electrodes modified with Cu electrodeposits, atomic force microscopy (AFM) images were also collected (Figure S2). AFM images of unmodified Cu (Figure S2A and S2B) show a relatively flat morphology. In contrast, the Cu electrode modified with the Cu electrodeposits are much rougher (Figure S2C and Figure S2D).

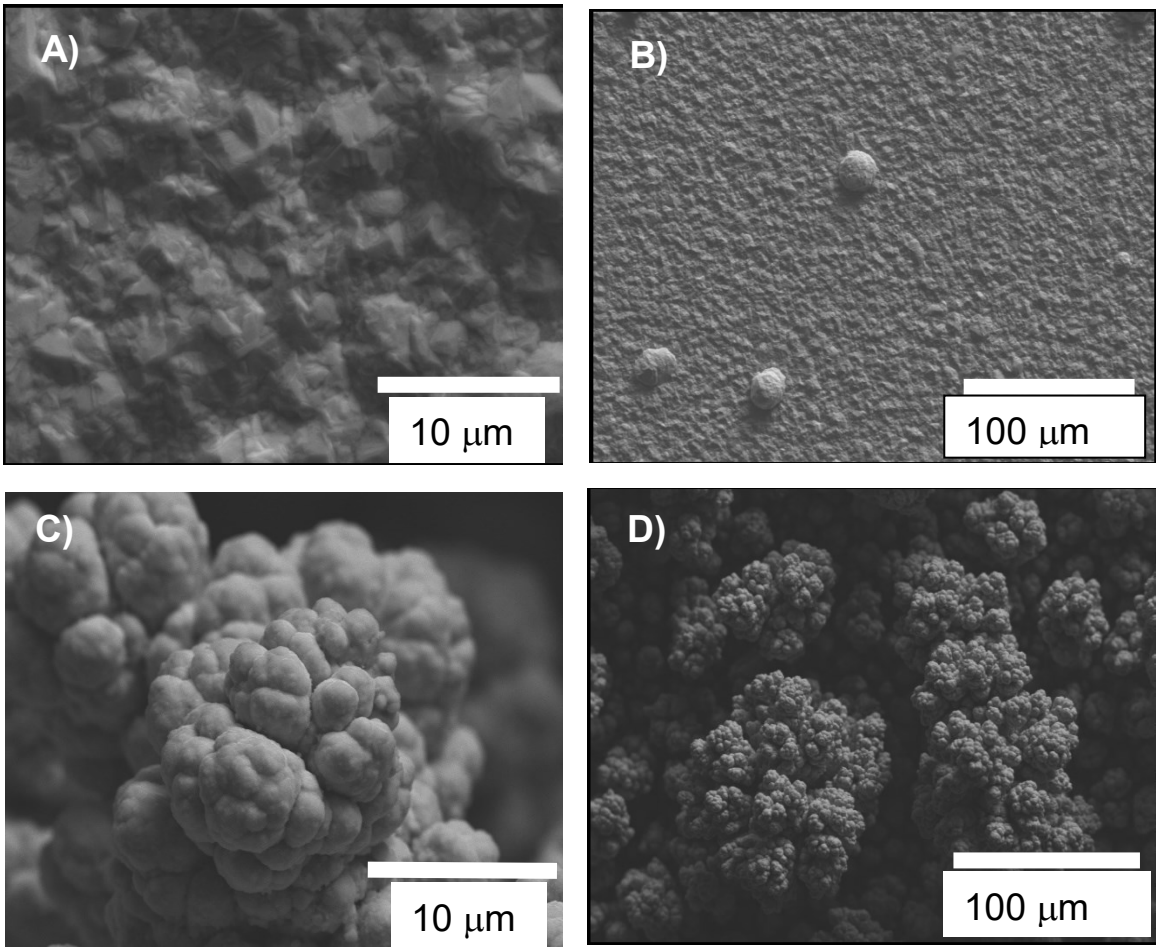

Figure 1: Top-down SEM images after 30 min of Cu electrodeposition on a Cu electrode using electrodeposition voltages of -0.14 V (A, B) and -0.5 V (C, D).

The electrochemically active surface areas of the electrodes with Cu electrodeposits were measured by conducting CVs in a solution containing $Ru(NH_3)_6Cl_3$ (Figure S1), a standard reversible redox couple ($E° = 0.10$ V vs. NHE). The more positive potential of ferrocene ($E° = 0.64$ V) compared to Cu ($E° = 0.34$ V) renders ferrocene unsuitable for this experiment because the Cu surface will be oxidized to Cu^{2+} at the potentials needed to observe the ferrocene couple.[38] By integrating the charge under the Ru^{3+}/Ru^{2+} couple for the flat unmodified Cu

electrode and comparing that value to the charge measured for the electrodes with Cu electrodeposits, the roughness factors and electrochemically active surface areas of these electrodes were determined. The roughness factors were calculated to be 1.84 and 4.92 for the electrodes with Cu electrodeposits formed at -0.14 V and -0.5 V, respectively. These measurements are consistent with the larger, rougher electrodeposits formed at -0.5 V as observed in the SEM images (Figure 1). Throughout the manuscript, we use the electrochemically active surface areas to calculate and report current densities.

The electrodes containing the Cu electrodeposits were also modified with a Nafion overlayer. Cross-sectional SEM-EDX images show that the Nafion overlayer forms a relatively uniform coating on the electrodeposited Cu surface with an approximate thickness of 6 μm (Figure S3A). This thickness of Nafion is chosen for all studies in this manuscript because previous results indicate that thinner or thicker layers result in lower NH_3 Faradaic efficiencies on flat Cu electrodes.[32] The EDX spectrum (Figure S3B) of the Nafion-modified electrodeposits confirms that the major elemental component is Cu. The other elements present are C, F, O, and S, which originate from the Nafion layer. EDX mapping demonstrates that Cu is present underneath the Nafion overlayer (Figure S3C), and F is localized in the Nafion overlayer (Figure S3D).

Electrode	**Water Contact Angle (degrees)**
Unmodified Cu	67 ± 5
Cu with electrodeposits formed using -0.14 V	55 ± 2
Cu with electrodeposits formed using -0.5 V	34 ± 5

Cu with electrodeposits formed using -0.14 V modified with Nafion	108 ± 1

Table 1: Water contact angles of various electrodes studied.

Water contact angles were measured to compare the hydrophobicity characteristics of the different Cu electrodes (Table 1). The angle between an unmodified Cu surface and a water droplet is (67 ± 5)°. For the Cu electrodes modified with Cu electrodeposits, the contact angles decreased relative to the flat surface. This result is expected because according to the Wenzel equation, a rough surface exhibits a lower contact angle compared to a corresponding flat surface when the water droplet is wetting (contact angle less than 90°).[39] The finding that the water contact angle for the electrodeposits formed at -0.5 V is less than the angle on the electrodeposits formed at -0.14 V is consistent with the increased surface roughness of the -0.5 V electrodeposits as determined by SEM and electrochemically active surface area measurements described previously. When the electrodeposits are modified with Nafion, the water droplets on both of the electrodeposits are non-wetting (contact angle greater than 90°). In these Nafion-modified cases, the contact angle for the -0.5 V electrodeposits is greater than that of the -0.14 V electrodeposits, which again is consistent with the relative surface roughness values because the Wenzel equation indicates that rougher non-wetting surfaces exhibit greater contact angles. Together with the cross-sectional SEM imaging, these results suggest that the Nafion layer form a relatively uniform coating over the Cu electrodeposits.

Electrocatalytic NO_3^- Reduction Activity and Product Distribution

Electrochemical NO_3^- reduction activities of different Cu electrodes were tested using LSV (Figure 2). The current densities for the LSVs and all subsequent current densities reported in this manuscript are normalized with respect to the electrochemically active surface areas of the

electrodes. The unmodified Cu electrode has a maximum current density of -0.57 mA cm^{-2} at -1 V and an onset potential (defined as the potential at which 10% of the maximum current density is attained) of -0.43 V. We electrodeposited Cu particles onto the Cu electrode with the aim of increasing the current density for the NO_3^- reduction reaction. The current density for the electrodes modified with Cu electrodeposits increases significantly as compared to unmodified Cu due in part to the increased surface area imparted the Cu electrodeposits (see previous discussion on roughness values and electrochemically active surface areas). Interestingly, the current density for the electrodes with Cu electrodeposits is still larger than that of the unmodified Cu even when taking into account the larger electrochemical active surface areas of the electrodes with electrodeposits (Figure 2, red and blue lines compared to Figure 2, black line). These results indicate that the Cu electrodeposits are intrinsically more kinetically active catalysts for NO_3^- reduction than unmodified Cu. The enhanced activity of the Cu electrodeposits is not directly related to the distribution of crystal faces in the electrode materials because the Cu electrodeposits formed at -0.14 V and -0.5 V have significantly different XRD spectra (*vide infra*). However, the electrodeposits likely possess more defects than flat Cu electrodes, and we therefore hypothesize that the enhanced current densities of the Cu electrodeposits originate from these defect sites.

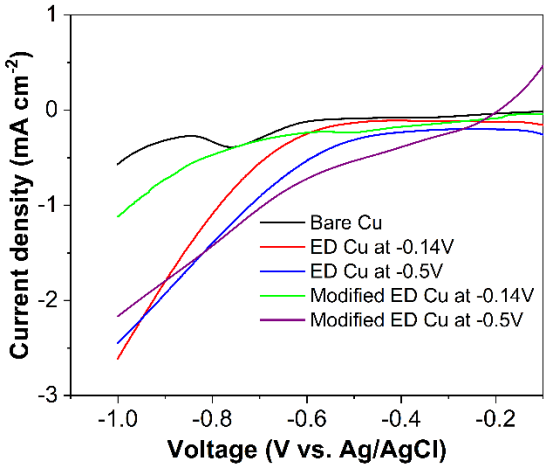

Figure 2: Linear sweep voltammograms in 50 mM $NaNO_3$ and 100 mM Na_2SO_4 at a scan rate of 10 mV s^{-1} of unmodified Cu (black line), Cu with Cu electrodeposits (ED) formed at -0.14 V (red line) or at -0.5 V (blue line), and Nafion-modified Cu with Cu electrodeposits formed at -0.14 V (green line) and at -0.5 V (purple line). The electrochemically active surface areas of the electrodes were used when calculating the current density.

After modifying the Cu electrodeposits with a 6 μm Nafion overlayer, the current density at -1.0 V decreases as compared to the Cu electrodeposits without Nafion (Figure 2, green line vs. red line and Figure 2, purple line vs. blue line). This decrease in current density likely occurs due to hindered mass transport of NO_3^- from the bulk solution to the electrode surface by the Nafion layer. Interestingly, the differences between the current densities at -1.0 V for the electrodeposits produced at -0.5 V is less than for the electrodeposits produced at -0.14 V. The exact origin of this difference is unknown, but it is likely related to differences in the morphologies of the electrodeposits in the two cases. Additionally, the onset potentials of the LSVs for the Nafion-modified electrodes for both the electrodeposits formed at -0.14 V and -0.5 V each shift positive compared to the corresponding electrodes without Nafion (Table S1). These positive shifts in onset potential upon addition of Nafion match previous experiments with Nafion-modified flat Cu electrodes and can be attributed to the activation of a Cu-NO intermediate through sulfonate groups on the Nafion, which increases the thermodynamic feasibility of NO_3^- reduction in the presence of Nafion.[32]

We next calculated the Faradaic efficiencies of NH_3 and NO_2^- production from NO_3^- electroreduction after 1 h chronoamperometry at -1.4 V using different Cu electrodes (Figures 3A and S4). The Faradaic efficiency of NH_3 production from an unmodified Cu electrode is (62 ± 2) % as reported before (Figure 3A, leftmost blue bar).[32] The Faradaic efficiency for NH_3 is similar for Cu with electrodeposits formed using -0.5 V, while the yield is slightly higher for the electrodeposits formed at -0.14 V (Figure 3A, three leftmost blue bars). Strikingly, after

modifying the electrodeposits formed at -0.14 V with a 6-μm-thick Nafion overlayer, the Faradaic efficiency for NH_3 production increases to (97.0 ± 0.3) %. This NH_3 yield is among the highest reported for NO_3^- reduction catalysts, making it one of the most selective electrocatalysts for NH_3 production (Table S2). Furthermore, this NH_3 Faradaic efficiency is significantly higher than the (91 ± 2) % obtained with a flat Cu electrode modified with Nafion. To study the effect of Nafion thickness on Cu electrodeposits formed at -0.14 V, we fabricated electrodes with Cu electrodeposits formed at -0.14 V modified with Nafion layers that are 3 μm, 8 μm, 10 μm, 12 μm, or 30 μm thick. The Faradaic efficiencies of NH_3 produced from these electrodes are 77%, 71%, 65%, 57%, and 5%, respectively. Because the 6-μm-thick Nafion layer exhibits the highest activity towards NH_3 production (97%), we used this Nafion thickness for the remaining studies in this manuscript.

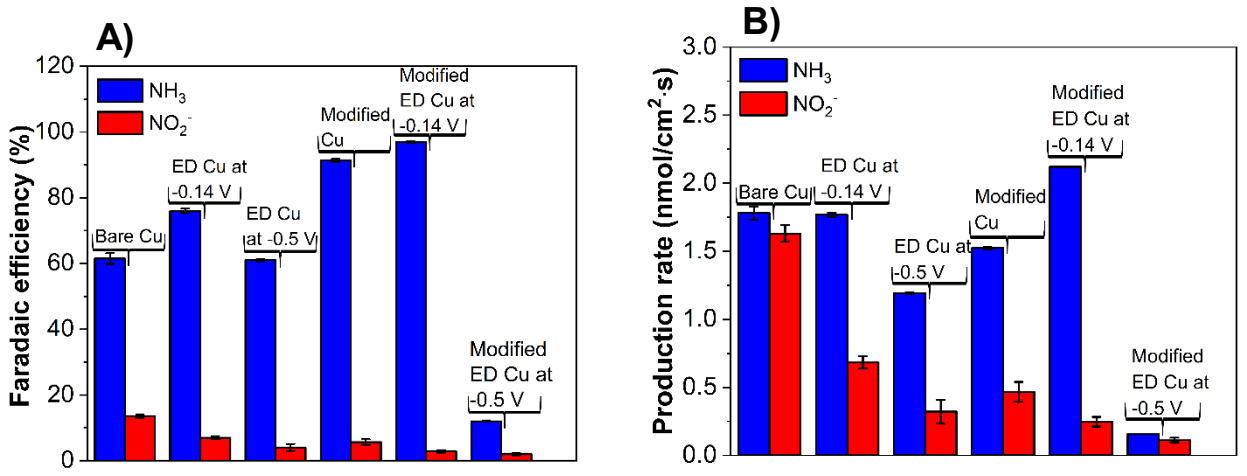

Figure 3: Faradaic efficiencies (A) and rate of production rate (B) of NH_3 (blue bars) and NO_2^- (blue bars) after 1 h of chronoamperometry at -1.4 V from unmodified (bare) Cu, Cu modified with electrodeposits (ED), and Cu modified with ED and Nafion. The electrochemically active surface areas of the electrodes were used when calculating the production rates.

Previous studies showed that the N-O bond in a Cu-NO intermediate is activated in the presence of Nafion. In particular, spectroscopic and density functional theory calculations indicate that the N-O bond length increases, which facilitates subsequent bond cleavage and NH_3 formation.[32] To evaluate the durability of the Nafion-modified Cu electrodeposits formed at -0.14 V, we performed chronoamperometry for 18 hours at -1.4 V (Figure S5). The NH_3 Faradaic efficiency for this long-term experiment was (85 ± 2) %, which indicates that the electrode is relatively stable over this time period and can support a high NH_3 Faradaic efficiency throughout the experiment.

Interestingly, the Faradaic efficiency for NH_3 production from Cu electrodeposits formed using -0.5 V drastically decreases to (11.1 ± 0.1) % upon Nafion modification unlike the electrodeposits formed at -0.14 V. The difference in NH_3 selectivity for the Nafion-modified electrodes with the two different electrodeposits could be due to differences in the crystal structure of the Cu electrodeposits as we will discuss later using XRD data. Figure 3B displays the NH_3 and NO_2^- production rates from the different Cu electrodes, and these production rates follow a similar trend as the Faradaic efficiencies.

Given the high NH_3 selectivity of the Nafion-modified electrode with Cu electrodeposits formed at -0.14 V, we focused on this electrode architecture for the remainder of our studies. In particular, we changed both the time employed to deposit the Cu particles and the voltage applied during the NO_3^- reduction reaction in an attempt to further optimize this system. Although increasing the electrodeposition time for generating the Cu electrodeposits increases the surface area of the electrodeposits, the NH_3 Faradaic efficiency significantly decreases (Figure S6), so we focused on the Nafion-modified electrode formed using only 30 min of electrodeposition.

We also assessed the effect of applied voltage on the electrocatalyst selectivity and kinetics (Figures 4 and S7). Increasing the magnitude of the cathodic voltage increases the NH_3 production rate per electrochemically active surface area of electrodes due to a greater applied overpotential (Figure 4B, blue bars). However, the NO_2^- production rates peak at -1.2 V, indicating that there is an optimal potential for NO_2^- generation (Figure 4B, red bars). At higher overpotentials, most of the NO_2^- produced at the electrode surface is converted to NH_3, which explains why the NO_2^- production rate decreases at more negative voltages. In terms of Faradaic efficiencies, the NO_2^- production decreases with increasing cathodic voltage with a corresponding rise in NH_3 Faradaic efficiency from -1 V to -1.4 V (Figure 4A). The NH_3 Faradaic efficiency decreases at voltages more negative than -1.4 V due to an increase in kinetically facile H_2 evolution at higher overpotentials.[35]

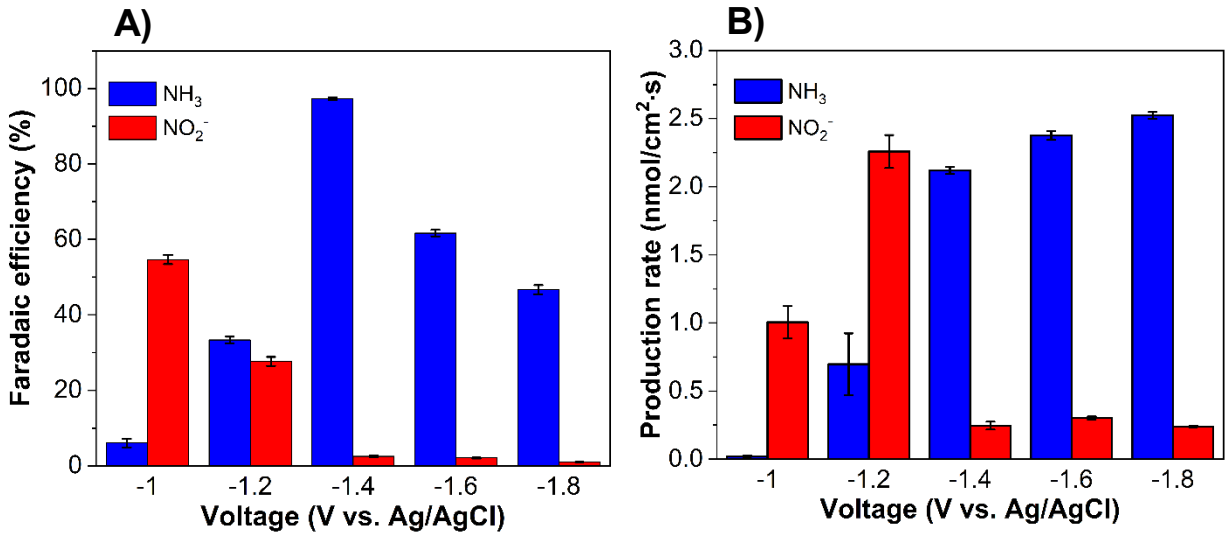

Figure 4: Faradaic efficiencies (A) and production rates (B) of NH_3 (blue bars) and NO_2^- (red bars) after 1 h of chronoamperometry at various voltages using Cu electrodes with Cu electrodeposits formed at -0.14 V modified with Nafion. The electrochemically active surface areas of the electrodes were used when calculating the production rates.

Mechanistic Studies of NO_3^- Reduction

To study the electrocatalytic NO_3^- reduction mechanism to produce NH_3, we performed three different chronoamperometry experiments using NO_3^-, NO_2^-, or NO-saturated electrolytes with the Cu electrodeposits formed at -0.14 V with and without Nafion modification (Figures S8 and S9). Faradaic efficiencies and rates of NH_3 production are reported in Figures 5A and 5B, respectively. In all three electrolytes, the NH_3 Faradaic efficiencies for the Nafion-modified electrode are significantly higher than those of the unmodified electrolyte. Furthermore, the Nafion-modified electrode exhibits high selectivity for NH_3 (> 90%) regardless of whether NO_3^-, NO_2^-, or NO is used as the precursor. These experiments suggest that both NO_2^- and NO are intermediates during NO_3^- reduction to NH_3 on the Nafion-modified Cu electrodeposits. A similar inference was discussed previously using flat Cu electrodes and is supported by surface-enhanced Raman spectroscopy and density functional theory calculations in our previous work.[32]

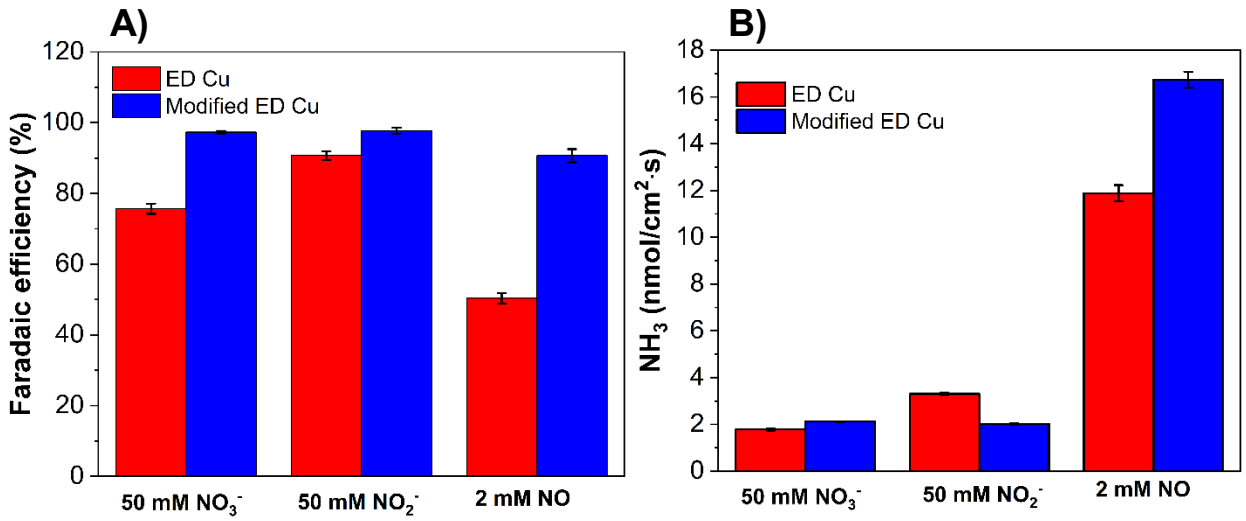

Figure 5: Faradaic efficiencies (A) and NH_3 production rates (B) from NO_3^- reduction (leftmost two bars), NO_2^- reduction (middle two bars), and NO reduction (rightmost two bars) using Cu electrodes with Cu electrodeposits (ED) formed at -0.14 V with (blue bars) and without (red bars) after 1 h of chronoamperometry at -1.4 V. The solutions used contained 100 mM Na_2SO_4 as a supporting electrolyte. The electrochemically active surface areas of the electrodes were used when calculating the production rates.

To understand the effect of electrodeposition voltage on the Cu electrodeposits, we performed XRD of the electrodeposits formed using -0.14 V and -0.5 V (Figure 6). In the

spectrum of the electrodeposits formed at -0.14 V, the (111), (200), (220), and (311) crystal faces are present, and the intensity of the (220) face is largest (Figure 6A). In contrast, the (111) facet exhibits the greatest intensity in the spectrum of the electrodeposits formed at -0.5 V (Figure 6B). Based on these results, we attribute the high Faradaic efficiency for NH_3 production with the Nafion-modified Cu electrodeposits formed at -0.14 V to the predominance of (220) faces in the Cu electrodeposits. Previous reports demonstrate that the Cu (111) face is the most active for the H_2 evolution reaction,[40] which for NO_3^- reduction catalysts would reduce the NH_3 Faradaic efficiency. Additionally, the (111) facet has the highest atomic packing density in face centered cubic systems and hence the fewest number of dangling bonds on the surface. We hypothesize that the higher coordination number of Cu in the (111) faces inhibits its activity towards NO_3^- reduction. This interpretation may explain why the Nafion-modified Cu electrodeposits formed at -0.5 V do not yield significant quantities of NH_3, while the Nafion-modified Cu electrodeposits formed using -0.14 V are highly selective for NH_3 generation.

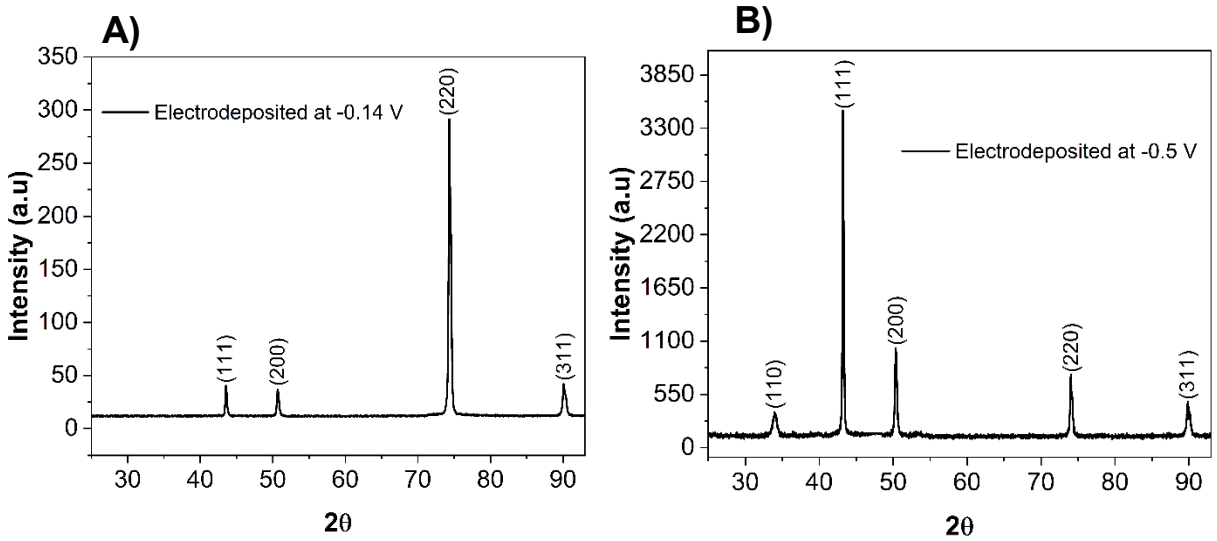

Figure 6: XRD spectra of Cu electrodes with Cu electrodeposits formed using -0.14 V (A) and -0.5 V (B).

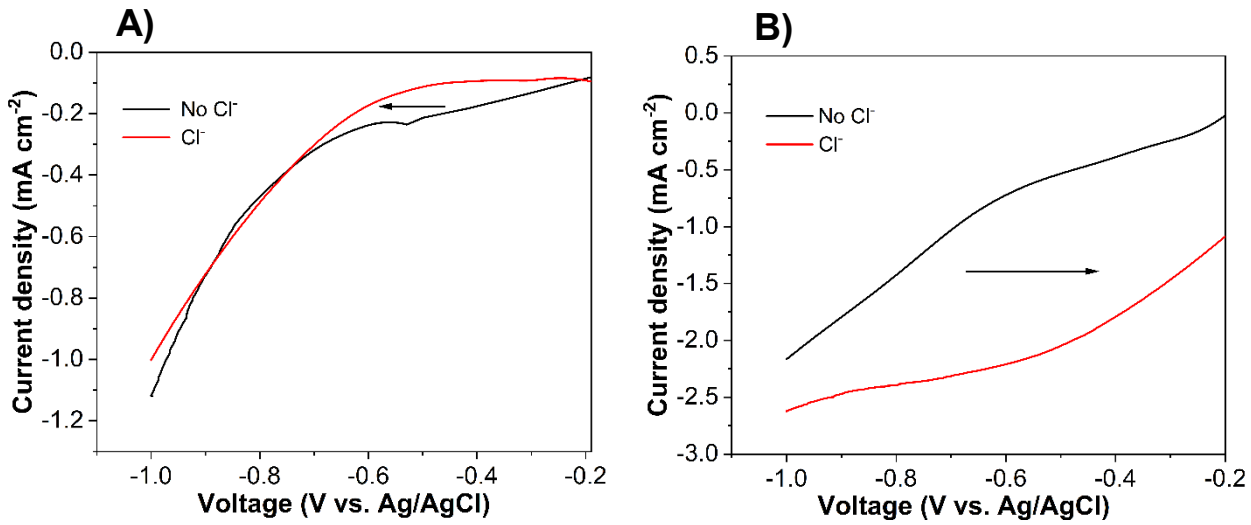

Figure 7: Linear sweep voltammograms at a scan rate of 10 mV s^{-1} of Nafion-modified Cu electrodes with Cu electrodeposits formed using -0.14 V (A) and -0.5 V (B) in 50 mM $NaNO_3$, 100 mM Na_2SO_4 (black line) and in 50 mM $NaNO_3$, 100 mM Na_2SO_4, and 10 mM NaCl (red line).

Through NO_3^- reduction experiments on Cu single crystals, Butcher Jr. and Gewirth previously determined that NO_3^- reduction leads to the partial oxidation of Cu surfaces during the catalytic cycle.[19] In particular, this oxidation facilitates NO_3^- reduction, and the reaction proceeds at lower overpotentials on crystal faces that are more readily oxidized. A corollary to this effect is that these same oxidizable crystal faces are poisoned by chloride because chloride etches copper oxides.[41] In the case of Cu electrodeposits, because the (220) face exhibits enhanced activity for NO_3^- reduction, we hypothesize that the electrodeposits formed using -0.14 V, which contain a predominance of the (220) face, would be poisoned by chloride as well. Indeed, a LSV of the Nafion-modified Cu electrodeposits formed using -0.14 V possesses an onset potential that is significantly shifted negative in a chloride-containing electrolyte (Figure 7A and Table S1). In

contrast, the less active Nafion-modified Cu electrodeposits formed using -0.5 V exhibit the opposite trend (Figure 7B and Table S1). Taken together, these results further suggest that the Cu (220) face is responsible for the enhanced NH_3 production of the Nafion-modified Cu electrodeposits formed using -0.14 V, which is likely facilitated by the formation of copper oxides on the surface during catalysis.

Conclusions

Although Nafion is commonly used as separator in two-compartment cells or as a binder in catalyst inks, here we modified Cu electrodeposits with a Nafion overlayer to enhance NH_3 production. Compared to previous reports using flat Cu electrodes, the Cu electrodeposits can both increase the NO_3^- reduction current density and the NH_3 Faradaic efficiency. In particular, the optimized catalyst reduces NO_3^- to NH_3 with a (97.0 ± 0.3) % Faradaic efficiency at a rate of (2.12 ± 0.01) nmol/cm^2-s. The structure and morphology of the electrodeposits were characterized using SEM-EDX, AFM, and XRD, and products were quantified in terms of electrochemically active surface areas. Along with the Nafion overlayer, the (220) face in the Cu electrodeposits suppresses H_2 evolution and enhances NH_3 yield. These studies will aid future researchers in rationally developing the next generation of active NO_3^- reduction electrocatalysts.

Supporting Information

Chronoamperometry data, SEM-EDX data, UV-visible spectroscopy data, and AFM data.

Author Information

Corresponding Author

Christopher J. Barile - *Department of Chemistry, University of Nevada, Reno, Reno, NV 89557, USA; orcid.org/0000-0002-4893-9506*; Email: cbarile@unr.edu

Authors

Profulla Mondol- *Department of Chemistry, University of Nevada, Reno, Reno, NV 89557, USA*

Jashmeen K. Thind- *Department of Chemistry, University of Nevada, Reno, Reno, NV 89557, USA*

Notes

The authors declare no completing financial interest.

Acknowledgments

This material is based upon work supported by the National Science Foundation CAREER Award under Grant No. CHE-2046105. SEM-EDS analysis was done in the Mackay Microbeam Laboratory at UNR, we acknowledge J. DesOrmeau for his kind assistance. We acknowledge the Shared Instrumentation Laboratory in the Department of Chemistry at UNR. The National Science Foundation (CHE-1429768) is acknowledged for the X-ray diffractometer.

References

1. Li, J.; Zhan, G.; Yang, J.; Quan, F.; Mao, C.; Liu, Y.; Wang, B.; Lei, F.; Li, L.; Chan, A. W. M. et al. Efficient Ammonia Electrosynthesis from Nitrate on Strained Ruthenium Nanoclusters. *J. Am. Chem. Soc.* **2020**, *142*, 7036–7046.
2. Cerrón-Calle, G. A.; Fajardo, A. S.; Sánchez-Sánchez, C. M.; Garcia-Segura, S. Highly Reactive Cu-Pt Bimetallic 3D-Electrocatalyst for Selective Nitrate Reduction to Ammonia. *Appl. Catal. B Environ.* **2022**, *302*, 120844-120853.
3. Wang, C.; Liu, Z.; Hu, T.; Li, J.; Dong, L.; Du, F.; Li, C.; Guo, C. Metasequoia-like Nanocrystal of Iron-Doped Copper for Efficient Electrocatalytic Nitrate Reduction into Ammonia in Neutral Media. *ChemSusChem* **2021**, *14*, 1825–1829.
4. Zhang, Y.; Chen, X.; Wang, W.; Yin, L.; Crittenden, J. C. Electrocatalytic Nitrate Reduction to Ammonia on Defective Au1Cu (111) Single-Atom Alloys. *Appl. Catal. B Environ.* **2022**, *310*, 121346-121356.

5. Wang, Y.; Zhou, W.; Jia, R.; Yu, Y.; Zhang, B. Unveiling the Activity Origin of a Copper-based Electrocatalyst for Selective Nitrate Reduction to Ammonia. *Angew. Chem. Int. Ed.* **2020**, *59*, 5350–5354.
6. Kyriakou, V.; Garagounis, I.; Vourros, A.; Vasileiou, E.; Stoukides, M. An Electrochemical Haber-Bosch Process. *Joule* **2020**, *4*, 142–158.
7. Wu, T.; Fan, W.; Zhang, Y.; Zhang, F. Electrochemical Synthesis of Ammonia: Progress and Challenges. *Mater. Today Phys.* **2021**, *16*, 100310-100332.
8. Kyriakou, V.; Garagounis, I.; Vasileiou, E.; Vourros, A.; Stoukides, M. Progress in the Electrochemical Synthesis of Ammonia. *Catal. Today* **2017**, *286*, 2–13.
9. Ertl, G. Primary Steps in Catalytic Synthesis of Ammonia. *J. Vac. Sci. Technol. A* **1983**, *1*, 1247–1253.
10. Jiao, F.; Xu, B. Electrochemical Ammonia Synthesis and Ammonia Fuel Cells. *Adv. Mater.* **2019**, *31*, 1805173-1805177.
11. Bhown, A.; Cussler, E. Mechanism for Selective Ammonia Transport through Poly (Vinylammonium Thiocyanate) Membranes. *J. Am. Chem. Soc.* **1991**, *113*, 742–749.
12. Guo, C.; Ran, J.; Vasileff, A.; Qiao, S.-Z. Rational Design of Electrocatalysts and Photo(Electro)Catalysts for Nitrogen Reduction to Ammonia (NH_3) under Ambient Conditions. *Energy Env. Sci* **2018**, *11*, 45–56.
13. Suryanto, B. H. R.; Du, H.-L.; Wang, D.; Chen, J.; Simonov, A. N.; MacFarlane, D. R. Challenges and Prospects in the Catalysis of Electroreduction of Nitrogen to Ammonia. *Nat. Catal.* **2019**, *2*, 290–296.
14. Wan, Y.; Xu, J.; Lv, R. Heterogeneous Electrocatalysts Design for Nitrogen Reduction Reaction under Ambient Conditions. *Mater. Today* **2019**, *27*, 69–90.

15. Tang, C.; Qiao, S.-Z. How to Explore Ambient Electrocatalytic Nitrogen Reduction Reliably and Insightfully. *Chem Soc Rev* **2019**, *48*, 3166–3180.
16. Badea, G. E. Electrocatalytic Reduction of Nitrate on Copper Electrode in Alkaline Solution. *Electrochimica Acta* **2009**, *54*, 996–1001.
17. Yang, J.; Sebastian, P.; Duca, M.; Hoogenboom, T.; Koper, M. T. M. PH Dependence of the Electroreduction of Nitrate on Rh and Pt Polycrystalline Electrodes. *Chem Commun* **2014**, *50*, 2148–2151.
18. Siriwatcharapiboon, W.; Kwon, Y.; Yang, J.; Chantry, R. L.; Li, Z.; Horswell, S. L.; Koper, M. T. M. Promotion Effects of Sn on the Electrocatalytic Reduction of Nitrate at Rh Nanoparticles. *ChemElectroChem* **2014**, *1*, 172–179.
19. Butcher, D. P.; Gewirth, A. A. Nitrate Reduction Pathways on Cu Single Crystal Surfaces: Effect of Oxide and Cl−. *Nano Energy* **2016**, *29*, 457–465.
20. Duca, M.; Klugt, B. van der; Hasnat, M. A.; Machida, M.; Koper, M. T. M. Electrocatalytic Reduction of Nitrite on a Polycrystalline Rhodium Electrode. *J. Catal.* **2010**, *275*, 61–69.
21. Zhang, X.; Wang, Y.; Liu, C.; Yu, Y.; Lu, S.; Zhang, B. Recent Advances in Non-Noble Metal Electrocatalysts for Nitrate Reduction. *Chem. Eng. J.* **2021**, *403*, 126269-126283.
22. Simpson, B. K.; Johnson, D. C. Electrocatalysis of Nitrate Reduction at Copper-Nickel Alloy Electrodes in Acidic Media. *Electroanal. N. Y. N* **2004**, *16*, 532–538.
23. Gao, J.; Jiang, B.; Ni, C.; Qi, Y.; Zhang, Y.; Oturan, N.; Oturan, M. A. Non-Precious Co_3O_4-TiO_2/Ti Cathode Based Electrocatalytic Nitrate Reduction: Preparation, Performance and Mechanism. *Appl. Catal. B Environ.* **2019**, *254*, 391–402.

24. McEnaney, J. M.; Blair, S. J.; Nielander, A. C.; Schwalbe, J. A.; Koshy, D. M.; Cargnello, M.; Jaramillo, T. F. Electrolyte Engineering for Efficient Electrochemical Nitrate Reduction to Ammonia on a Titanium Electrode. *ACS Sustain. Chem. Eng.* **2020**, *8*, 2672–2681.

25. Jia, R.; Wang, Y.; Wang, C.; Ling, Y.; Yu, Y.; Zhang, B. Boosting Selective Nitrate Electroreduction to Ammonium by Constructing Oxygen Vacancies in TiO_2. *ACS Catal.* **2020**, *10*, 3533–3540.

26. Martínez, J.; Ortiz, A.; Ortiz, I. State-of-the-Art and Perspectives of the Catalytic and Electrocatalytic Reduction of Aqueous Nitrates. *Appl. Catal. B Environ.* **2017**, *207*, 42–59.

27. Fu, X.; Zhao, X.; Hu, X.; He, K.; Yu, Y.; Li, T.; Tu, Q.; Qian, X.; Yue, Q.; Wasielewski, M. R. et al. Alternative Route for Electrochemical Ammonia Synthesis by Reduction of Nitrate on Copper Nanosheets. *Appl. Mater. Today* **2020**, *19*, 100620-100625.

28. Wang, C.; Liu, Y.; Schmid, R. Rapid Nonovershooting Control for Simultaneous Infusion of Anesthetics and Analgesics. *IFAC-Pap.* **2021**, *54*, 1–6.

29. Nørskov, J. K.; Bligaard, T.; Rossmeisl, J.; Christensen, C. H. Towards the Computational Design of Solid Catalysts. *Nat. Chem.* **2009**, *1*, 37–46.

30. Machida, M.; Sato, K.; Ishibashi, I.; Hasnat, M. A.; Ikeue, K. Electrocatalytic Nitrate Hydrogenation over an H^+-Conducting Solid Polymer Electrolyte Membrane–Modified Cathode Assembly. *Chem. Commun.* **2006**, No. 7, 732–734.

31. Hasnat, M. A.; Ishibashi, I.; Sato, K.; Agui, R.; Yamaguchi, T.; Ikeue, K.; Machida, M. Electrocatalytic Reduction of Nitrate Using Cu–Pd and Cu–Pt Cathodes/H+-Conducting Solid Polymer Electrolyte Membrane Assemblies. *Bull. Chem. Soc. Jpn.* **2008**, *81*, 1675–1680.

32. Mondol, P.; Panthi, D.; Albarran Ayala, A. J.; Odoh, S. O.; Barile, C. J. Membrane-Modified Electrocatalysts for Nitrate Reduction to Ammonia with High Faradaic Efficiency. *J Mater Chem A* **2022**, *10*, 22428–22436.
33. Kay, J. G. Inorganic Chemistry: Handbook of Preparative Inorganic Chemistry. Vol. 1. Georg Brauer, Ed. Translated from the German Edition (Stuttgart, Ed. 2, 1960) by Scripta Technica. Reed F. Riley, Ed. Academic Press, New York, **1964**, *144*, 703–703.
34. Zacharia, I. G.; Deen, W. M. Diffusivity and Solubility of Nitric Oxide in Water and Saline. *Ann. Biomed. Eng.* **2005**, *33*, 214–222.
35. Chen, G.-F.; Yuan, Y.; Jiang, H.; Ren, S.-Y.; Ding, L.-X.; Ma, L.; Wu, T.; Lu, J.; Wang, H. Electrochemical Reduction of Nitrate to Ammonia via Direct Eight-Electron Transfer Using a Copper–Molecular Solid Catalyst. *Nat. Energy* **2020**, *5*, 605–613.
36. Schnetger, B.; Lehners, C. Determination of Nitrate plus Nitrite in Small Volume Marine Water Samples Using Vanadium (III) Chloride as a Reduction Agent. *Mar. Chem.* **2014**, *160*, 91–98.
37. Schlesinger, M.; Paunovic, M. *Modern Electroplating*; John Wiley & Sons: Hoboken, NJ, 2011.
38. Mondol, P.; Barile, C. J. Four-Electron Electrocatalytic O_2 Reduction by a Ferrocene-Modified Glutathione Complex of Cu. *ACS Appl. Energy Mater.* **2021**, *4*, 9611–9617.
39. Wolansky, G.; Marmur, A. Apparent Contact Angles on Rough Surfaces: The Wenzel Equation Revisited. *Colloids Surf. Physicochem. Eng. Asp.* **1999**, *156*, 381–388.
40. Santos, E.; Pötting, K.; Lundin, A.; Quaino, P.; Schmickler, W. Hydrogen Evolution on Single-Crystal Copper and Silver: A Theoretical Study. *ChemPhysChem* **2010**, *11*, 1491–1495.

41. Touzé, E.; Cougnon, C. Study of the Air-Formed Oxide Layer at the Copper Surface and Its Impact on the Copper Corrosion in an Aggressive Chloride Medium. *Electrochim. Acta* **2018**, *262*, 206–213.

TOC Graphic

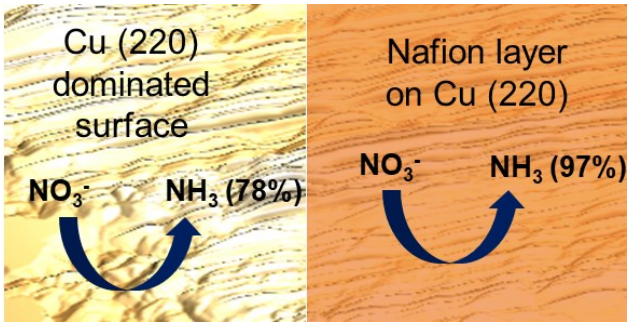
Cu (220) dominated surface
NO_3^-
NH_3 (78%)
Nafion layer on Cu (220)
NO_3^-
NH_3 (97%)